

Article

Short-Term Hydro-Thermal-Solar Scheduling with CCGT Based on Self-Adaptive Genetic Algorithm

Borche Postolov ^{1,*}, Nikolay Hinov ^{2,*} , Atanas Iliev ¹ and Dimitar Dimitrov ¹

¹ Faculty of Electrical Engineering and Information Technologies, Ss. Cyril and Methodius University, Ruger Boshkovikj 18, P.O. Box 574 Skopje, North Macedonia

² Faculty of Electronic Engineering and Technologies, Technical University of Sofia, 8 Kl. Ohridski Blvd, 1000 Sofia, Bulgaria

* Correspondence: borche.postolov@hotmail.com (B.P.); hinov@tu-sofia.bg (N.H.)

Abstract: This paper presents a new metaheuristic approach based on a self-adaptive genetic algorithm (SAGA) for solving the short-term hydro-thermal-solar scheduling with combined-cycle (CCGT) units. First of all, the proposed approach is applied to a test system with different characteristics, considering the valve-point effect. The simulation results obtained from the new SAGA are compared with the results obtained from some other metaheuristic methods, such as AIS, DE, and EP to reveal the validity and verify the feasibility of the proposed approach. The test results show that the proposed metaheuristic approach proves the effectiveness and superiority of the SAGA algorithm for solving the short-term hydro-thermal-solar scheduling (SHTSS) problem.

Keywords: hydrothermal scheduling; genetic algorithm; self-adaptive penalty; Laplace crossover; MPTM mutation



Citation: Postolov, B.; Hinov, N.; Iliev, A.; Dimitrov, D. Short-Term Hydro-Thermal-Solar Scheduling with CCGT Based on Self-Adaptive Genetic Algorithm. *Energies* **2022**, *15*, 5989. <https://doi.org/10.3390/en15165989>

Academic Editor: Javier Contreras

Received: 20 July 2022

Accepted: 14 August 2022

Published: 18 August 2022

Publisher's Note: MDPI stays neutral with regard to jurisdictional claims in published maps and institutional affiliations.



Copyright: © 2022 by the authors. Licensee MDPI, Basel, Switzerland. This article is an open access article distributed under the terms and conditions of the Creative Commons Attribution (CC BY) license (<https://creativecommons.org/licenses/by/4.0/>).

1. Introduction

In the recent period, the electric power demand has increased and fossil fuel prices have risen, which has led to growing the world energy crisis. Therefore, the world has tended to reduce the use of TPP by using renewable energy sources to reduce the emissions and harmful gases that are released from TPP. These harmful gases harm the environment, and this leads to an increase in the temperature of the planet, which causes global warming. Accordingly, the European Union has introduced stricter directives, which provide for the decommitment of TPP, and a gradual increase in the renewable penetrations in the system [1–3].

Therefore, the incorporation of the short-term hydrothermal generation scheduling (STHS) problem and new renewable energy integration has great importance in the power system operation [4]. The STHS problem is one of the most important optimization problems in power system planning. The primary goal of the STHS problem is to determine the optimal power-generation schedule of the TPP and HPP to minimize the total operation cost of the system. On other hand, the total operating costs and flexibility of the TPP's operation can be favorably influenced by committing combined cycle gas turbines (CCGT) into the system and the appropriate decommitment of existing conventional TPPs, especially in the transition period, which has already begun. However, in SHTSS, one of the basic features of solar power plants (SPP) is the extreme variability and unpredictability of the output power, primarily due to the dependence on weather conditions [5].

These two attributes are especially evident in modern power systems, in which solar power plants have an increasing penetration. In addition to this, modern PV modules use bifacial technology [5], so their orientation significantly affects the output power of the solar power plant and, thus, all the parameters of the system (including costs). According to what has been said so far, it can be said that this paper deals with the impact of the orientation of

the modules on the total operating costs. This analysis is of particular importance for the integration of SPP in the power system.

2. Motivation, Literature Review, and Contributions

To solve the SHTS problem, various approaches are applied based on the achievements of applied mathematics and mathematical software, and, initially, various classical optimization methods were proposed, such as the dynamic programming method [6,7], the Lagrange relaxation method [8,9], and mixed integer programming [10,11]. In this aspect, it is known that the considered optimization methods are difficult to apply in solving complex optimization problems. On the other hand, gradient methods are characterized by fast convergence but are inefficient and of limited applicability to problems that are described by nonconvex and discontinuous objective functions, such as the SHTSS problem.

In articles [12–17], techniques based on application of artificial intelligence are considered: evolutionary programming, simulated annealing, differential evolution, artificial neural network, genetic algorithm (GA), and particle swarm optimization (PSO) for solving of the SHTS optimization problem. A characteristic of these manuscripts is that only a quadratic objective function is used and, also, significantly simpler constraints. Thus, the SHTS optimization problem has become more complex by incorporating the valve point load and transmission loss into the objective function while considering various hydro, thermal, system, and security constraints.

In this regard, it is known that, when applying metaheuristic approaches to solve optimization problems such as SHTS, there is a significantly greater possibility of avoiding local minima and obtaining an optimal global approach. Due to the widespread distribution of decentralized power systems, the hydrothermal scheduling has been widely studied by researchers worldwide.

In previous studies, some of the considered algorithms failed to obtain optimal solutions when considering various complex constraints based on multi-objective tasks. An excellent real-coded genetic algorithm (RCGA) solution was obtained by introducing a self-adaptive penalty function, Laplace crossover, and Makinen, Perriot, and Toivanen (MPTM) mutation. Thus, the planning problem is more accurately described based on the formulation of constraints inherent in the operation of a real system, such as reservoir storage capacity constraints, water discharge constraints, available production constraints, generator constraints, ramp rate constraint, valve point effect, and transmission line constraint.

All optimization methods strive to obtain the global optimum, but gradient methods easily become stuck in local optima. GA has proven to be a better method of obtaining the global optimum because it works with a population which performs diversification and intensification of the search space, i.e., a group of solutions, compared to gradient methods, which work with a single solution.

In this article, a new constraint handling technique is proposed through the fitness function evaluation by a new self-adaptive penalty, Laplace crossover, and adaptive crossover and mutation strategy. A newly proposed constraint handling repair mechanism has been proposed for consideration of the constraints that are most difficult to satisfy, especially the power balance constraint and the hydro constraints. The main contributions of this paper are:

- A new self-adaptive penalty for constraints handling, which require no tuning.
- A new crossover technique, i.e., Laplace crossover, which has a self-adaptive tuning ability, which is important to maintain population diversity.
- A new constraint handling repair mechanism for simultaneous satisfaction of all constraints, especially power balance and hydraulic continuity equation, which are neglected in other papers. This allows for a significantly more physically realistic solution.

- Analysis of the influence of the orientation of the modules on the output power of the solar power plant and, thus, on the overall system parameters. This is especially important for system operators, as they receive future scenarios for operational planning. Therefore, they will be able to decide on the maximum installed power of solar power plants in the system.
- The paper is of particular importance to the academic community, as it presents a scenario in operational planning in a “green energy transition”, with a slow departure from coal, i.e., in a period of committing CCGTs, decommissioning TPP, and solar power plants taking an increasing penetration.
- An additional advantage of the proposed approach is that it can be used to create a graphical user interface (GUI) that can be developed and enhanced. Having a GUI is a very important tool for system operators in operational planning and real-time operational decision making.

3. Problem Formulation

3.1. Combined Cycle Gas Turbines

TPP with combined cycle gas turbines (CCGT), shown in Figure 1, has a gas and steam turbine. The main purpose of such plants is to use the heat generated at the outlet of the gas turbine. Since the exhaust gases coming out of the gas turbine have extremely high temperatures, about 600 °C can be used as a means to heat water and produce steam for the steam turbine. This increases the efficiency of the process itself, as the heat that would otherwise be lost is used for further steam production. The efficiency of such a plant reaches up to 60%. In a CCGT, the compressor compresses the air and sends it to the combustion chamber, where the combustion fuel is supplied at the same time.

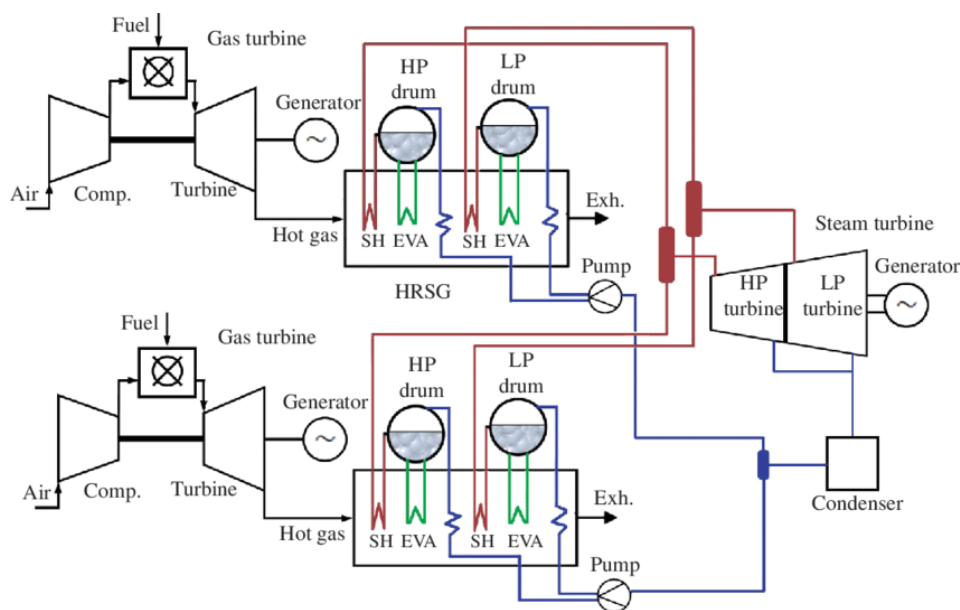


Figure 1. CCGT with two GTs and one ST.

Very high-temperature combustion gases are led from the combustion chamber to the gas turbine, where they expand, giving useful work on the shaft connected to the gas turbine rotor. The shaft drives the generator and produces electricity that is sent to the grid.

After expansion, the exhaust gases from the gas turbine are led to the heat recovery steam generator (HRSG). There is still a lot of unused air at the output of the gas turbine, and this excess air is used to burn additional fuel in the HRSG. In the HRSG, the feed water is heated to evaporation and overheats to the set parameters. The superheated steam goes from the HRSG to the steam turbine, where it expands and hands over the mechanical work to the electric generator. After that, the steam, now of low parameters,

goes to the condenser, where it condenses. After condensation, the water is returned to the HRSG by the feed pump for reheating. It has already been mentioned that, with this principle, we increase the usability of the whole process, by changing CCGT’s operation mode, which is shown in Figure 2 [17], i.e., the optimal output power, according to the daily load diagram [18,19].

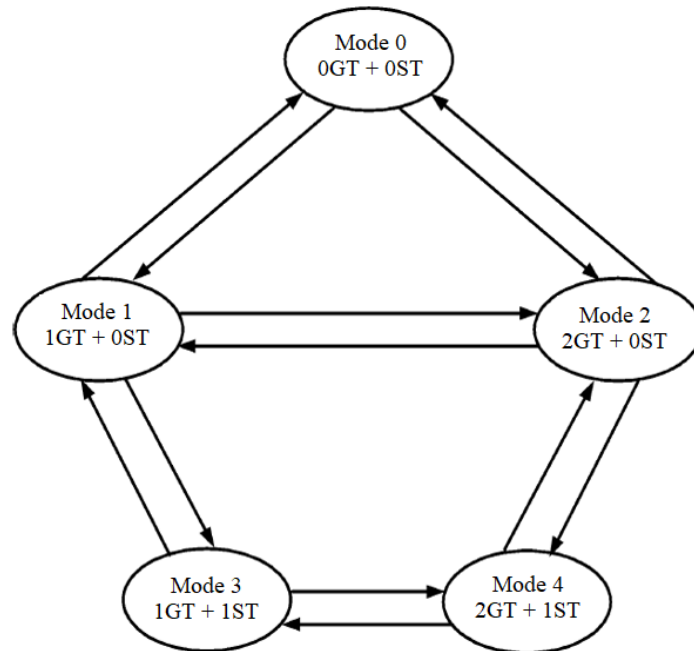


Figure 2. State transition diagram for CCGT with two GTs and one ST [17].

3.2. Objective Function

The main objective in solving the SHTSS optimization problem is to minimize fuel costs in the thermal power plants (TPPs). In this regard, fuel costs in HPPs are neglected, as the ongoing costs of hydropower generation systems are significantly lower compared to other production costs, such as thermal energy. In this way, the optimal fuel costs are determined for the electricity generation from the TPPs. When using an optimization procedure in modern power systems, the main objective is to minimize the total fuel cost by properly using renewable energy sources, such as SPPs, while providing the demand power for the whole optimization period, which, in SHTSS, is one day, i.e., 24 h. It should be noted that, firstly, the units are committed according to [18–20] (considering various constraints), and then the SHTSS problem is solved.

The fuel costs of TPPs are usually represented by a quadratic function and depend on the generator output power. Therefore, the objective function of the problem is the sum of the fuel costs of all TPPs that are subject to optimization, i.e., [21–23]:

$$\min F = \sum_{j=1}^J \sum_{t=1}^{NT} [F_{t,j} \cdot j] \cdot u_{t,j} \tag{1}$$

$$\forall t \in NT; j \in J; u \in \{0, 1\}$$

where u represents the commitment state of TPP t at interval j (0 for a decommitted unit or 1 for a committed unit). On other hand, $F_{t,j}$ is the fuel cost function of the TPP t and is represented by the nonconvex function:

$$F_{t,j} = a_t + b_t \cdot P_{GTt,j} + c_t \cdot P_{GTt,j}^2 + \left| d_t \sin(e_t (P_{GTt}^{\min} - P_{GTt,j})) \right| \tag{2}$$

$$\forall t \in NT; j \in J$$

where $a_t, b_t, c_t, d_t,$ and e_t represent cost coefficients of the TPP t , and P_{GTt}^{\min} is the technical minimum, while j is the index of the optimization interval.

3.3. Constraints

3.3.1. Generator Constraint

The generation output power of TPPs and HPPs is enclosed in the technical minimum and the technical maximum, and is represented by:

$$\begin{aligned} u_{t,j}P_{GTt}^{\min} &\leq P_{GTt,j} \leq u_{t,j}P_{GTt}^{\max} \\ u_{h,j}P_{GHh}^{\min} &\leq P_{GHh,j} \leq u_{h,j}P_{GHh}^{\max} \end{aligned} \tag{3}$$

3.3.2. Power Balance Constraint

The total output power from all TPP (including CCGT), HPP, and SPP must be equal to the total load and losses in the system:

$$\sum_{t=1}^{NT} u_{t,j}P_{GTt,j} + \sum_{h=1}^{NH} u_{h,j}P_{GHh,j} + \sum_{s=1}^{NS} u_{s,j}P_{GSs,j} = P_{P,j} + P_{L,j} \tag{4}$$

$$\begin{aligned} P_{L,j} &= \sum_{i=1}^{NG} \sum_{j=1}^{NG} P_{Gi}B_{ij}P_{Gj} + \sum_{j=1}^{NG} B_{i0}P_{Gj} + B_{00} \\ \forall i \in NG; j \in NG; NG &= NT + NH \end{aligned} \tag{5}$$

3.3.3. Spinning Reserve Constraint

The required level of spinning reserve, which is required for the system security, is given as:

$$\sum_{i=1}^{NT+NH} u_{i,j}P_{Gi}^{\max} \geq (P_{P,j} + P_{L,j} + R); \forall j \in J; u \in \{0,1\} \tag{6}$$

while the required spinning reserve is calculated according to the empirical formula of ENTSO (UCTE), i.e., [24]:

$$R = \sqrt{a_{res} \cdot P_{P,max} + b_{res}^2} - b_{res}; a_{res} = 10 \text{ MW}; b_{res} = 150 \text{ MW} \tag{7}$$

where a_{res} and b_{res} represent empirical constants, and $P_{P,max}$ the system's peak load.

Thus, the spinning reserve constraint with available spinning reserve from TPPs and HPPs is represented by:

$$\begin{aligned} \sum_{t=1}^{NT} u_{t,j}P_{GTt}^{AV} &\geq R_T \\ \sum_{h=1}^{NH} u_{h,j}P_{GHh}^{AV} &\geq R_H \end{aligned} \tag{8}$$

where $P_{GT,t}^{AV}$ and $P_{GH,h}^{AV}$ are the available spinning reserve of TPP t or HPP h ; R_T is the total required spinning reserve of TPPs; and R_H is the totally required spinning reserve of HPPs. It is considered that $R_T = 0.75R$ and $R_H = 0.25R$.

3.3.4. Ramp Rate Constraint

The sudden change in the output power of the generators is limited by the ramp rate constraint, i.e.,

$$\begin{aligned} P_{GTt,j} &= \max(P_{GTt}^{\min}, (P_{GTt,j} - DRT_t)) \\ P_{GHh,j} &= \max(P_{GHh}^{\min}, (P_{GHh,j} - DRH_h)) \end{aligned} \tag{9}$$

$$\begin{aligned} P_{GTt,j} &= \min(P_{GTt}^{\max}, (P_{GTt,j} + URT_t)) \\ P_{GHh,j} &= \min(P_{GHh}^{\max}, (P_{GHh,j} + URH_h)) \end{aligned} \tag{10}$$

where $URT_t, DRT_t, URH_h,$ and DRH_h represent the allowable upper and down rates of TPP t or HPP h .

3.3.5. Transmission Line Constraint

The maximum power that can be transmitted by a transmission line is represented by the following constraint:

$$|P_{\text{line},g}| \leq P_{\text{line},g}^{\max}, \quad g = 1, \dots, G \quad (11)$$

where G is the total number of transmission lines in the system. The active power of the transmission line is obtained by power flow calculation by applying the DC model, i.e., DC power flow [20].

3.3.6. Water Availability Constraint

The total water discharge is physically constrained by a total available volume i.e.,

$$\sum_{j=1}^J Q_{th,j} \cdot T_j \leq V_{h,k} \quad (12)$$

where T_j is the duration of interval j , Q_{th} is the water discharge, i.e., the input–output curve of the HPP, and is represented by a quadratic function:

$$Q_{th}(P_{GH,h}) = \alpha_h + \beta_h \cdot P_{GH,h} + \gamma_h \cdot P_{GH,h}^2 \quad (13)$$

where $P_{GH,h}$ is the output power of HPP h , and α_h , β_h , and γ_h are constant coefficients of the input–output curve.

3.3.7. Available Production Constraint

The available production of TPPs is defined according to the following expression:

$$\sum_{i=1}^{NT+NH} P_{Gi,j} \cdot T_j = W_{\max,i} \quad (14)$$

The available production of HPPs is defined according to the available (initial) volume V_k and the total discharge time T_{dis} , i.e.,

$$Q_{\max,h} = Q_{\text{ins},h} = f(\alpha_h, \beta_h, \gamma_h, P_{GH,h}^{\max}) \quad (\text{m}^3/\text{h}) \quad (15)$$

$$T_{\text{dis},h} = \frac{V_{k,h}}{Q_{\max,h}} \quad (\text{h}) \quad (16)$$

$$W_{\max,h} = P_{GH,h}^{\max} \cdot T_{\text{dis},h} \quad (\text{MWh}) \quad (17)$$

3.3.8. Dynamic Balance of the Reservoir Storage

Reservoir storage of HPP is compressed by spillage and inflow at the preceding event and it must track the continuity equations of the hydraulic system at each time interval j , and it is described as follows:

$$V_{h,j} = V_{h,(j-1)} + I_{h,j} - Q_{th,j} - S_{h,j} \quad (18)$$

where $V_{h,j}$ is the storage volume of HPP h ; $I_{h,j}$ is the inflow in reservoir h ; and $S_{h,j}$ is the water spillage of the reservoir h . In this paper, water spillage is neglected.

3.3.9. Initial and Final Reservoir Storage Constraint

The volume constraints of the reservoir at the beginning and end of the scheduling period are determined by:

$$\begin{aligned} V_{h,0} &= V_h^{\text{initial}} \\ V_{h,24} &= V_h^{\text{end}} \end{aligned} \quad (19)$$

3.3.10. Water Discharge Constraint

The water discharge constraint is determined by:

$$Q_h^{\min} \leq Q_{h,j} \leq Q_h^{\max} \quad (20)$$

3.3.11. Reservoir Volume Constraint

The physical limitation of reservoir volume is given by:

$$V_h^{\min} \leq V_{h,j} \leq V_h^{\max} \quad (21)$$

4. Genetic Algorithm

4.1. Initialization

The initial population is modeled based on the optimal solution, previously obtained from unit commitment (as conducted in reference [20]), as follows:

$$\begin{aligned} P_{G0,m}^a &= (1 - \psi) \cdot P_{GUC,m}; P_{G0,m}^b = (1 + \psi) \cdot P_{GUC,m} \\ P_{n,m} &= P_{G0,m}^a + \text{rand} \cdot (P_{G0,m}^b - P_{G0,m}^a) \\ n &= 1, \dots, N_{\text{pop}}; m = 1, \dots, N_{\text{var}} = (NT + NH) \cdot J \end{aligned} \quad (22)$$

where ψ is the diversity factor and has a value of 0.2.

4.2. Fitness Function Evaluation and Constraint Handling

The initial population contains 200 chromosomes. To increase the robustness of the algorithm but also to maintain the quality of the initial population, before the main stage of the algorithm, the best 100 chromosomes are selected. This selection is made according to the following expression [25,26]:

$$F(x) = \begin{cases} f(\mathbf{X}) & \text{if } \mathbf{X} \text{ is feasible} \\ f_{\max} + \left[\sum_{i=1}^I \langle g_i(\mathbf{X}) \rangle + \sum_{k=1}^K |h_k(\mathbf{X})| \right] & \text{if } \mathbf{X} \text{ is infeasible} \end{cases} \quad (23)$$

where f_{\max} is the value of the objective function of the worst feasible solution, i.e., chromosome in the population.

In this paper, a new constraints handling technique is proposed for fitness function evaluation by a new self-adaptive penalty function, which has not been applied to this type of optimization problem so far. It consists of distance function $d(X)$ and penalty function $p(X)$. The proposed technique works only with inequality constraints, i.e., [27–30]:

$$G_i(X) = \begin{cases} \max[g_i(X), 0], i = 1, \dots, I \\ \max[|h_k(X)| - \varepsilon, 0], k = I + 1, \dots, K \end{cases} \quad (24)$$

and, after that, the final fitness function receives a self-adaptive value (but not the sum of the objective function and classical penalty function):

$$F(X) = d(X) + p(X) \quad (25)$$

$$d(\mathbf{X}) = \begin{cases} v(\mathbf{X}), \text{ if } r_f = 0 \\ \sqrt{[f''(\mathbf{X})]^2 + [v(\mathbf{X})]^2}, \text{ otherwise} \end{cases} \quad (26)$$

$$v(\mathbf{X}) = \frac{\sum_{i=1}^m w_i(G_i(\mathbf{X}))}{\sum_{i=1}^m w_i} \quad (27)$$

$$f''(\mathbf{X}) = \frac{f(\mathbf{X}) - f_{\min}}{f_{\max} - f_{\min}} \quad (28)$$

$$p(\mathbf{X}) = (1 - r_f)M(\mathbf{X}) + r_fN(\mathbf{X}) \quad (29)$$

$$M(\mathbf{X}) = \begin{cases} 0, & \text{if } r_f = 0 \\ v(\mathbf{X}), & \text{otherwise} \end{cases} \quad (30)$$

$$N(\mathbf{X}) = \begin{cases} 0, & \text{if } \mathbf{X} \text{ is a feasible} \\ f''(\mathbf{X}), & \text{if } \mathbf{X} \text{ is an infeasible} \end{cases} \quad (31)$$

where, $w_i = 1/G_{\max,i}$ is a weight parameter; $G_{\max,i}$ is the maximum value for violation of constraint $G_i(\mathbf{X})$ recorded thus far; and $v(\mathbf{X})$ is the total constraint violation. The main advantage of the proposed algorithm is that, unlike the static penalty, the self-adaptive penalty does not require parameter setting.

4.3. Selection

To prevent premature convergence, the fitness function is scaled linearly. The relationship between the original fitness function and the scaled one is given by the expression:

$$\begin{aligned} f_s &= a_s f + b_s \\ a_s &= (sp - 1)f_{av} / (f_{\max} - f_{\min}) \\ b_s &= (1 - a_s)f_{av} \end{aligned} \quad (32)$$

where sp is a parameter that controls the selection pressure and is in the interval (1.2–2), f_s is the scaled fitness value, F is the fitness value, f_{av} is the mean fitness of the population, f_{\max} and f_{\min} are the maximum and minimum fitness value in the current population, and a_s and b_s are scaling coefficients [31–33].

4.4. Crossover

For the proposed SAGA, Laplace crossover (LX) was applied. Two offspring are generated from a pair of parents, as described. First, a uniformly distributed random number α_L is generated, so $\alpha_L \in [0, 1]$. Then, a random number β_L is calculated, which follows the Laplace distribution by simply inverting the distribution function of the Laplace distribution, i.e., [34]:

$$\beta_L = \begin{cases} a_L - b_L \ln(\alpha_L), & \alpha_L \leq 0.5 \\ a_L + b_L \ln(\alpha_L), & \alpha_L > 0.5 \end{cases} \quad (33)$$

The offspring are given by the equations:

$$\begin{aligned} y_i^{(1)} &= x_i^{(1)} + \beta_L \left| x_i^{(1)} - x_i^{(2)} \right| \\ y_i^{(2)} &= x_i^{(2)} + \beta_L \left| x_i^{(1)} - x_i^{(2)} \right| \end{aligned} \quad (34)$$

4.5. Mutation

In the newly proposed self-adaptive genetic algorithm (SAGA), the Makinen, Periaux, and Toivanen mutation (MPTM) is applied (which is originally proposed by Makinen [35] and is applied for a general optimization problem). In this paper, MPTM is applied for the first time to that optimization problem. The implementation of MPTM in SAGA consists of the following. First, an evenly distributed random number r is generated, such that $r \in [0, 1]$. Then, the new mutated chromosome \hat{x} is calculated as follows:

$$\hat{x} = (1 - \hat{p})x^{(l)} + \hat{p}x^{(u)} \quad (35)$$

$$\hat{p} = \begin{cases} p - p \left(\frac{p-r}{p} \right)^b & \text{if } r < p \\ p & \text{if } r = p \\ p + (1-p) \left(\frac{r-p}{1-p} \right)^b & \text{if } r > p \end{cases} \quad (36)$$

$$p = \frac{x - x^{(l)}}{x^{(u)} - x} \quad (37)$$

where $x^{(l)}$ and $x^{(u)}$ are the upper bound and the lower bound, respectively.

4.6. Adaptive Crossover and Mutation Strategy

The target of the newly proposed crossover and mutation strategies is to regulate the crossover and mutation probability of the chromosome, and thus maintain population diversity. These strategies are based on the difference between its fitness function and the average fitness function of the population [20], i.e.,

$$P_c = \begin{cases} k_1(f_{\max} - f_c)/(f_{\max} - f_{\text{av}}), & f_c \geq f_{\text{av}} \\ k_2, & f_c < f_{\text{av}} \end{cases} \quad (38)$$

$$P_m = \begin{cases} k_3(f_{\max} - f_c)/(f_{\max} - f_{\text{av}}), & f_c \geq f_{\text{av}} \\ k_4, & f_c < f_{\text{av}} \end{cases} \quad (39)$$

where $k_1 < 1$, $k_2 < 1$, $k_3 < 1$, and $k_4 < 1$. The values of the k parameters, i.e., k_1 , k_2 , k_3 , and k_4 , were obtained by the “trial and error” method. Because these parameters regulate the crossover and mutation probability, a large number of simulations were performed on a suitable test system, and then results are compared with the results of other proposed algorithms. Taking into account that these parameters significantly affect the performance of the algorithm and the CPU time, an optimal interval is determined, which represents a balance between the quality of the results (the global optimum) and the CPU time, so it is recommended $0.8 \leq k_1 \leq 1$; $0.17 \leq k_2 \leq 0.22$; and $0.94 \leq k_3 \leq 1$; $0.14 \leq k_4 \leq 0.18$. In this paper, $k_1 = 0.95$, $k_2 = 0.20$, and $k_3 = 1$, $k_4 = 0.18$.

4.7. Elitism Strategy

In this paper, an elitism strategy is proposed by creating a combined population that consists of the best 50 parents and the best 50 children. This combined population represents the population for the next generation. Figure 3 shows the simplified block diagram of the SAGA, while Algorithms 1–3 represent different parts of the newly proposed constraint handling repair mechanism.

Algorithm 1: New constraints handling for reservoir storage volume (initial and final reservoir storage)

- 1: Set $V_1^{\text{end}} = v \cdot 10^4$; $V_2^{\text{end}} = v \cdot 10^4$;
 - 2: Set $\varepsilon_h = 0.1$; $iter_{\max} = 7$; $j_{\min} = 1$; $j_{\max} = ND$; $iter = 1$;
 - 3: **while** $h \leq NH$
 - a. $\Delta V_h = V_h^{\text{initial}} + \sum_{j=1}^J I_{h,j} - \sum_{j=1}^J Q_{h,j} - V_h^{\text{end}}$
 - b. **if** $(|\Delta V_h| \leq \varepsilon_h)^{j=1}$ **or** $(iter \geq iter_{\max})$ **then**
 - i. $j_{\text{rand}} = \text{randi}([j_{\min} \ j_{\max}], 1, 1)$
 - ii. $Q_{h,j_{\text{rand}}} = \max(Q_h^{\min}, (\min(Q_{h,j_{\text{rand}}} + \Delta V_h, Q_h^{\max})))$
 - c. **else**
 - i. $Q_{h,j} = [Q_{h,1} \ Q_{h,2} \ \dots \ Q_{h,24}]$
 - ii. $Q_{h,j} = \max(Q_h^{\min}, (\min(Q_{h,j} + \Delta V_h / ND, Q_h^{\max})))$
 - iii. $iter = iter + 1$
 - d. **end if**
 - 4: **end while**
-

Algorithm 2: New constraints handling for constraints handling for water discharge

```

1: for  $h=1:NH$ 
  a. for  $j=1:ND$ 
    i. if  $Q_{h,j} < Q_h^{\min}$  then
      1.  $Q_{h,j} = Q_h^{\min}$ 
    ii. elseif  $Q_{h,j} > Q_h^{\max}$  then
      1.  $Q_{h,j} = Q_h^{\max}$ 
    iii. end if
  b. end for
2: end for

```

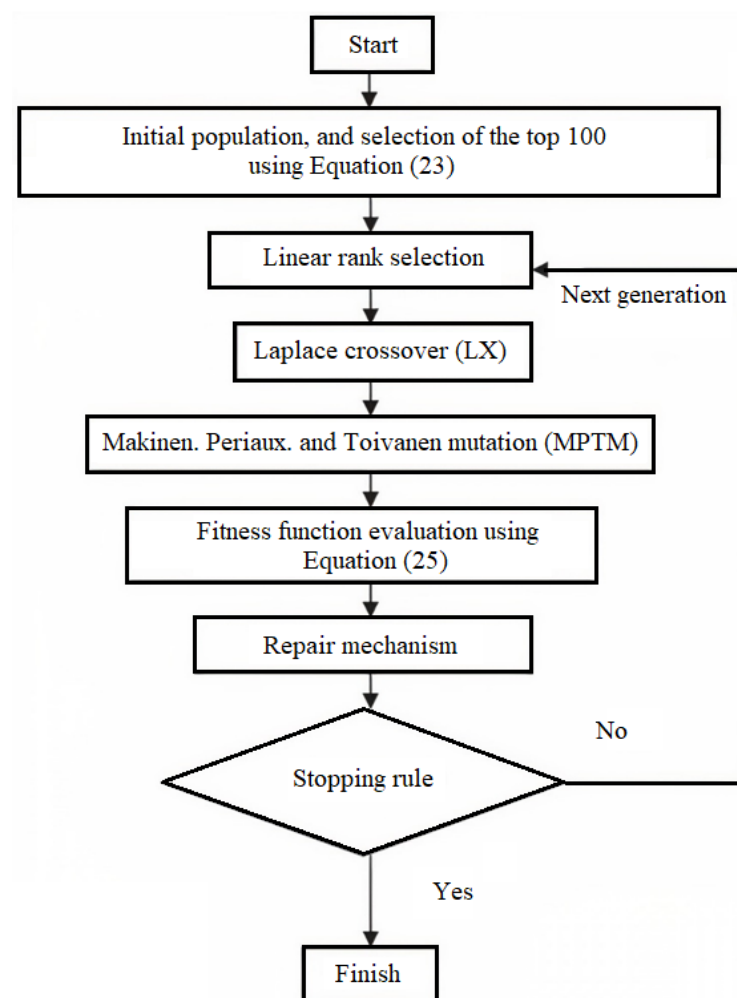


Figure 3. Simplified flowchart of the proposed SAGA.

Algorithm 3: New constraints handling for real power balance and ramp rate.

```

1: for  $i = 1: NH$ 
  a. for  $j = 1: J$ 
    i. if  $P_{GH}(i, j) \neq 0$  then
      1. if  $P_{GH}(i, j) \leq \max(P_{GH}^{\min}(i), (P_{GH}(i, j) - DRH(i)))$  then
        a.  $P_{GH}(i, j) = \max(P_{GH}^{\min}(i), (P_{GH}(i, j) - DRH(i)))$ 
      2. elseif  $P_{GH}(i, j) \geq \min(P_{GH}^{\max}(i), (P_{GH}(i, j) + URH(i)))$ 
        a.  $P_{GH}(i, j) = \min(P_{GH}^{\max}(i), (P_{GH}(i, j) + URH(i)))$ 
      3. end if
    ii. end if
  b. end for
2: end for
3: for  $j = 1: J$ 
  a.  $WH_{\text{new}}(j) = \sum P_{GH}(i, j)$ 
  b.  $P_{PT}(j) = P_p(\bar{j}) + P_L(j) - WH_{\text{new}}(j)$ 
4: end for
5:  $P_L(j) = \sum_{m=1}^{NT+NH} \sum_{n=1}^{NT+NH} P_{G,m}(j) \cdot B_{mn} \cdot P_{G,n}(j) + \sum_{m=1}^{NT+NH} B_{m0} P_{Gm} + B_{00}$ 
6: for  $j = 1: J$ 
  a.  $\Delta P_{PT}(j) = \sum P_{GT}(t, j) - P_{PT}(j) - P_L(j)$ 
  b. while  $|\Delta P_{PT}^{l-1}(j)| > 10^{-3}$ 
    i.  $\Delta P_{PT, \text{mean}}(j) = \Delta P_{PT}(j) / NT$ 
    ii. for  $t = 1: NT$ 
      1. if  $P_{GT}(t, j) \neq 0$  then
        a.  $P_{GT}(t, j) = P_{GT}(t, j) - \Delta P_{PT, \text{mean}}(j)$ 
        b. if
           $P_{GT}(t, j) \leq \max(P_{GT}^{\min}(t), (P_{GT}(t, j) - DRT(t)))$ 
          then
            i.  $P_{GT}(t, j) = \max(P_{GT}^{\min}(t), (P_{GT}(t, j) - DRT(t)))$ 
          c. elseif
           $P_{GT}(t, j) \geq \min(P_{GT}^{\max}(t), (P_{GT}(t, j) + URT(t)))$ 
          then
            i.  $P_{GT}(t, j) = \min(P_{GT}^{\max}(t), (P_{GT}(t, j) + URT(t)))$ 
          d. end if
        2. end if
      3.  $\Delta P_{PT}(j) = \sum_{t=1}^{NT} P_{GT}(t, j) - P_{PT}(j) - P_L(j)$ 
    iii. end for
  c. end while
7: end for

```

4.8. Computational Procedure

The computational procedure of the newly proposed SAGA is shown in Figure 3, and is briefly described as follows:

Step 1: Preparation and initialization. Determine the necessary computational parameters of the algorithm. Generate the initial population from the previous UC solution, perform fitness function evaluation using Equation (24), and select the top 100 chromosomes.

Step 2: Calculate the fitness function values and total constraint violation of each chromosome in the parent population using Equations (25)–(31). Then, determine the elite chromosome.

Step 3: Apply a linear rank selection. Each chromosome in the population is ranked in increasing order of fitness function, from 1 to n . Linear ranking assigns a selection probability to each chromosome that is proportional to the individual's rank.

Step 4: LX and MPTM is used to generate the offspring population. To enhance the population diversity and prevent premature convergence, before the predefined crossover operator and mutation operator, an appropriate strategy will be applied. These strategies regulate the crossover and mutation probability, based on the fitness deviation of the chromosome from the mean fitness function of the entire population.

Step 5: Fitness function evaluation. Calculate the fitness function values and total constraint violation of each chromosome.

Step 6: Determine constraint violations, and then apply the new constraint handling repair mechanism, in order for the chromosome to be feasible again.

Step 7: Apply an elitism strategy. The parent population and offspring population are combined in one group. They are then sorted based on the fitness function in descending order. Then, the better, i.e., best 100 chromosomes, will be chosen as the members in the new generation.

Step 8: Repeat steps 3 to 7 until the maximum number of generations is reached, then export the optimal solution, i.e., chromosome.

5. Simulation Experiment and Result Analysis

5.1. Test System 1

The investigated system consists of two TPPs and two HPPs, and the effect of the valve point is considered in the simulation. The data for conducting the numerical experiments were taken from [36]. Table 1 shows the optimal generation of the studied system. In the performed simulations, the population size and maximum generations are 100 and 500, respectively, as shown in [37].

Table 1. Optimal generation scheduling of the test system [37].

Interval	P_{GT1} (MW)	P_{GT2} (MW)	P_{GH1} (MW)	P_{GH2} (MW)
1	181.14	264.66	400.00	85.11
2	300.00	340.23	400.00	217.02
3	140.76	309.24	400.00	300.00

In the simulations, the spin reserve is chosen to be 10% of the total load demand. Table 2 presents a comparison of the results for the test system using different optimization methods, which was obtained in the authors' previous research [37]. In the particular example, the experiment was conducted 50 times. Thus, the average fuel costs were obtained based on the data from conducting 50 experiments.

Table 2. Optimal generation scheduling of the test system [37].

	SAGA	GA ¹	AIS [30]	DE [30]	EP [30]	AIS [30]
FT (EUR)	47,184	66,341	66,117	66,121	66,198	−40.12 (%)
CPU time (s)	6.03	28.53	53.43	60.76	75.48	−47.4 (s)
STD (EUR)	26,861	-	-	-	-	-

¹ This means that generation scheduling is obtained with Classical GA (modeled by the author, neglecting all newly proposed techniques from SAGA), to represent the difference between GA and SAGA [32].

5.2. Test System 2

In this subchapter, the efficiency of the first part of the proposed algorithm, i.e., the unit commitment part, will be verified. For this purpose, the algorithm will be applied to a test system, which consists of six thermal power plants. All data, such as unit characteristics and load demand, are taken from [38,39]. On an Intel Core i7-9750H CPU@2.60GHZ with 16GB RAM, 50 independent simulations were made for a relevant comparison with other methods. Table 3 shows the total fuel costs for test system 2.

Table 3. Optimal generation scheduling of the test system 2 [38,39].

	Best (EUR)	Average (EUR)	Worst (EUR)	Change (%)
DA-PSO [38]	13,292.28	-	-	-
PSO-GWO [39]	13,600.00	-	-	-
GA	13,221.55	13,288.19	13,321.57	-
SAGA	13,126.31	13,171.69	13,193.28	-1.264
Newton's method	-	13,170.68	-	-
Difference SAGA—Newton	-	-	-	0.0077

- This means that generation scheduling is obtained with Classical GA (modeled by the author, neglecting all newly proposed techniques from SAGA), to represent the difference between GA and SAGA.

5.3. IEEE 30 Bus System

The performance of the proposed algorithm, after its verification, has been evaluated using the Modified IEEE 30 bus system. This system consists of 30 buses, 7 generators, i.e., four TPP (buses 1, 2, 5, and 8), of which TPP1 (in bus 1) is with CCGT, two HPP (buses 11 and 13), and one SPP (bus 10), and 41 transmission lines. The data for this system are taken from [38,40–43]. The data for inflows in reservoirs 1 and 2 are taken from [20]. The data for CCGT TPP are shown in Tables 4 and 5 and are taken from [44]. A spinning reserve value of 10% of the system's peak load is selected. When solving the optimization problem, 75% of the spinning reserve was chosen to be covered by TPPs, and the remaining 25% by HPPs. Figure 4 shows the daily load diagram of the system, and Figure 5 shows its single-line diagram. For an IEEE 30 bus system, the proposed approach runs for 50 independent simulations, and the population size and maximum number of iterations are set to 100 and 500, respectively.

Table 4. Composition data for CCGT.

Mode	Composition	GT	ST	$p_{GT,t}^{\min}$ (MW)	$p_{GT,t}^{\max}$ (MW)	UR_t (MW)	DR_t (MW)
0	0 + 0	0	0	0	0	0	0
1	1 + 0	1	0	20	80	60	60
2	2 + 0	2	0	40	160	120	120
3	1 + 1	1	1	30	135	105	105
4	2 + 1	2	1	50	215	165	165

Table 5. Cost curve coefficients data for CCGT.

Mode	Composition	a_t	b_t	c_t	d_t	e_t
0	0 + 0	0	0	0	0	0
1	1 + 0	169.92700	2.36929	0.00051	18	0.037
2	2 + 0	339.85400	2.36929	0.00025	18	0.037
3	1 + 1	149.39630	1.40033	0.00063	18	0.037
4	2 + 1	247.06916	1.53006	0.00036	18	0.037

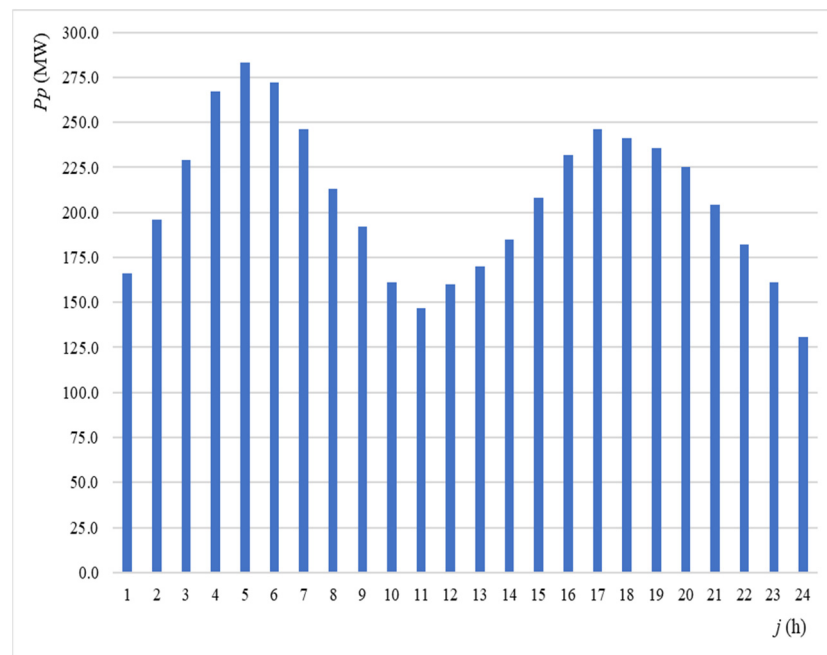


Figure 4. Daily load diagram of the IEEE 30 bus system.

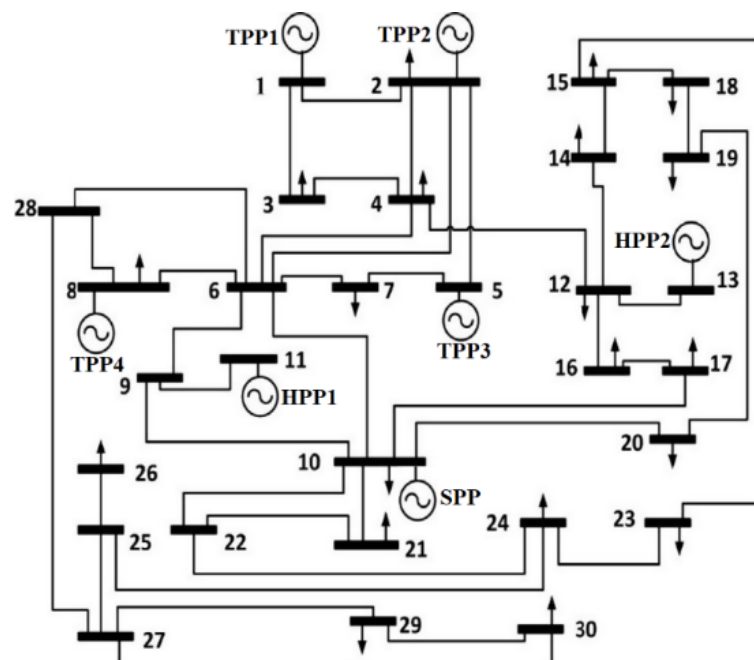


Figure 5. Single-line diagram of the modified IEEE 30 bus system.

5.3.1. Solar Power Plant Model

The SPP model was developed in the PVSYST software package. It implements 34,000 Trina Solar bifacial 500 Wp PV modules and 170 grid-tie inverters of the type Fronius International—Tauro Eco 100-3-P, with a modeled DC/AC ratio of 1.00. The SPP consists of 2125 strings and has an installed power of 17 MWp. The albedo of the substrate is 0.7, and the height above ground is 1.5 m. The data for PV modules are taken from [45].

To prove the initial hypothesis, i.e., that the orientation and location of the SPP affect the total fuel costs, two SPP (i.e., cases) are modeled. In case 1, the location of the SPP is Gaag, Netherlands (latitude: 51.96° and longitude: 4.29), while, in case 2, the location of the SPP is Bitola, Macedonia (latitude: 41.03° and longitude: 21.33). Given the HUPX's

electricity price diagram, which is shown in Figure 6 [46], each of these two cases involves three different sub-cases. In other words, the electricity price diagram has two peaks, one in the morning and the other in the afternoon. To achieve the greatest possible energy balance (largest production in the morning or afternoon), in two of the three sub-cases, the orientation of the modules, i.e., the azimuth, will be 90° and -90° .

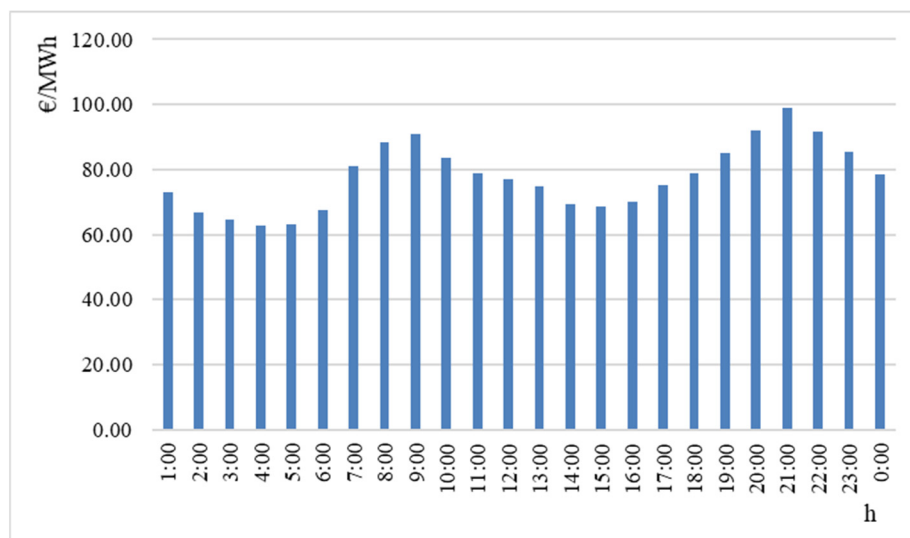


Figure 6. HUPX's electricity price diagram for the chosen optimization period (9 June 2021).

The parameters for both cases are shown in Tables 6 and 7. The best values of parameters, such as height above ground sheds spacing, injected energy per year (E_{GRID}), and tilt angle, are obtained through “trial and error”.

Table 6. Data for case 1: Gaag, Netherlands.

Sub-Case	Tilt Angle (°)	Azimuth (°)	Height (m)	Sheds Spacing (m)	Albedo	E_{GRID} (MWh)
1	25	0	1.5	9	0.7	20,457
2	20	90	1.5	12	0.7	18,883
3	20	-90	1.5	12	0.7	18,734

Table 7. Data for case 2: Bitola, Macedonia.

Sub-Case	Tilt Angle (°)	Azimuth (°)	Height (m)	Sheds Spacing (m)	Albedo	E_{GRID} (MWh)
1	25	0	1.5	9	0.7	28,620
2	20	90	1.5	12	0.7	26,448
3	20	-90	1.5	12	0.7	26,481

Figure 7 shows the output power of the SPP for case 1, and Figure 8 shows the output power for case 2 for the specific optimization period, i.e., 9 June 2021.

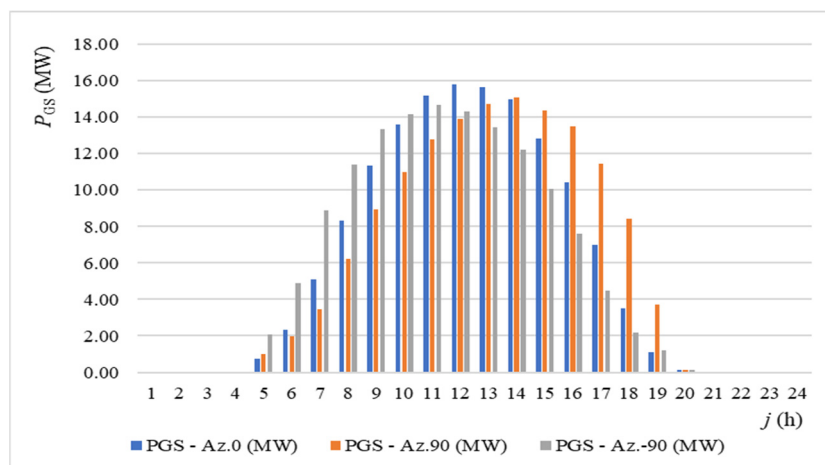


Figure 7. Daily output power of the SPP for case 1.

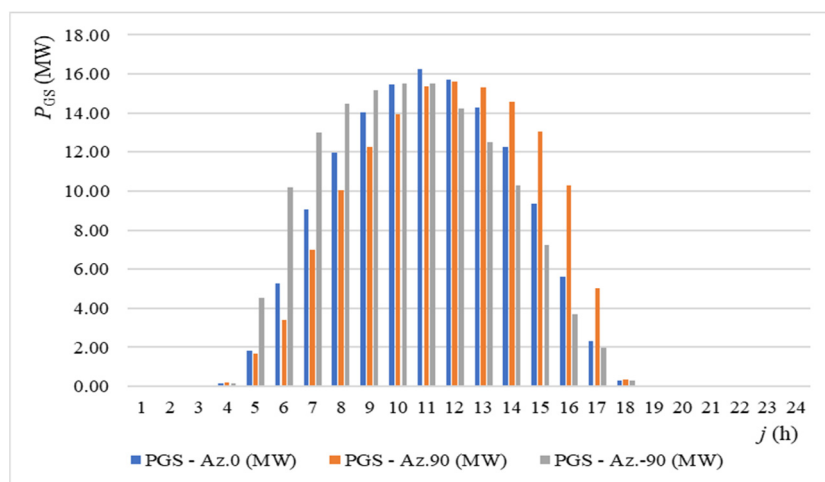


Figure 8. Daily output power of the SPP for case 2.

From Tables 6 and 7, it can be seen that the annual production for case 2 is significantly higher than the production for case 1. This should not come as a surprise, given the fact that the global horizontal radiation for case 2 is 1480.3 kWh/m², while, for case 1, it is 1040.0 kWh/m², meaning case 2 is 1.42 times higher compared to case 1.

5.3.2. Case 1: Gaag, Netherlands

Obtained heat rate (HR) for all TPPs, including the CCGT, is given in Table 8. The average value of total fuel cost for all sub-cases, obtained using the proposed method is shown in Table 9, and the computation time taken by the algorithm is 21.28 s. The average fuel costs are obtained from 50 independent simulations. Figure 9, Figure 10, and Figure 11, respectively, show the optimal output power of TPPs and HPPs for sub-case 1, 2, and 3, while the optimal generation scheduling for the optimization period for the lowest cost sub-case, using the proposed optimization algorithm, is shown in Figure 10 and in Table 10.

Table 8. Obtained HR for TPPs (EUR/MW).

	CCGT-Mode1	CCGT-Mode2	CCGT-Mode3	CCGT-Mode4	$P_{GT,2}$	$P_{GT,3}$	$P_{GT,4}$
HR	4.71	4.64	2.68	2.77	3.27	4.24	3.83

Table 9. Total fuel cost for case 1.

	Sub-Case 1	Sub-Case 2	Sub-Case 3
<i>FT</i> (EUR)	10,316.19	10,255.34	10,320.99
Relative change compared to sub-case 2 (%)	0.59	-	0.63

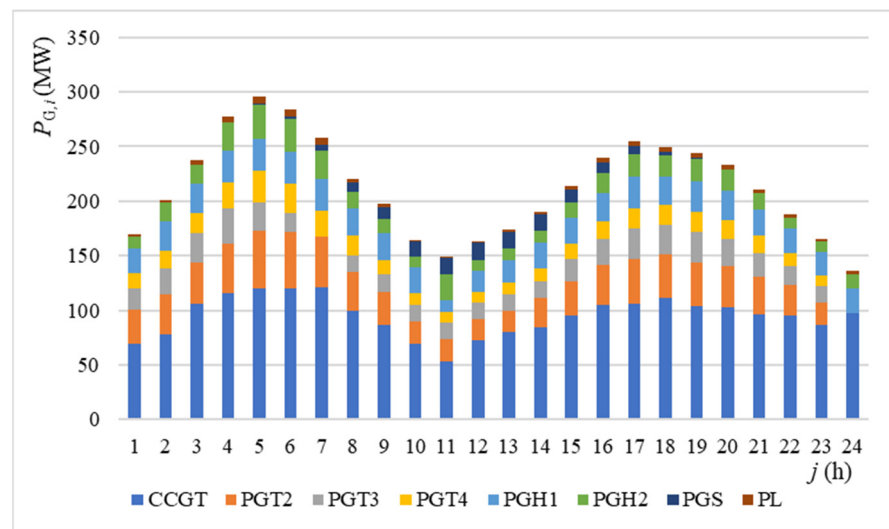


Figure 9. Optimal generation scheduling for case 1–sub-case 1.

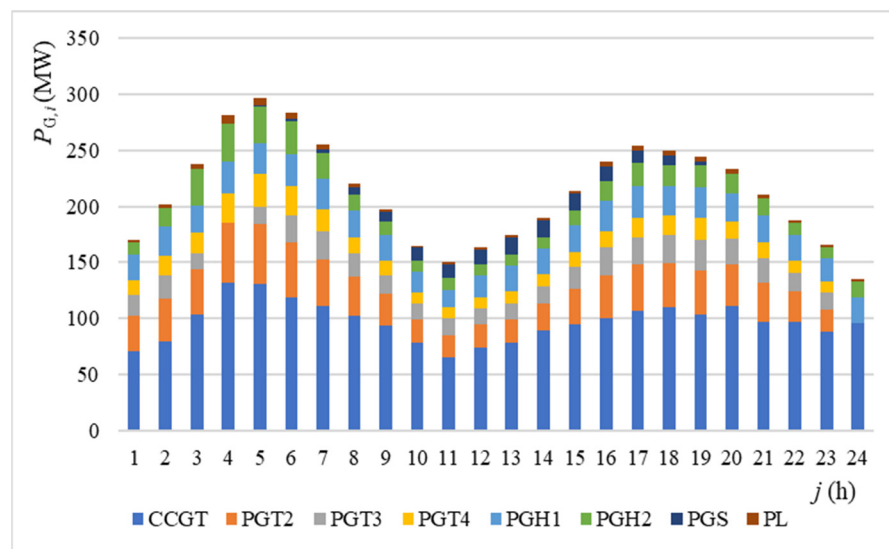


Figure 10. Optimal generation scheduling for case 1–sub-case 2.

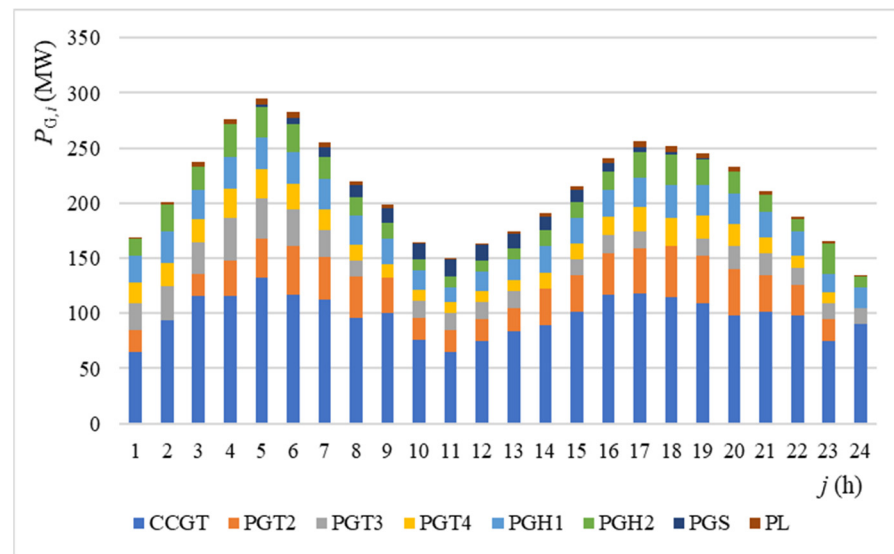


Figure 11. Optimal generation scheduling for case 1-sub-case 3.

Table 10. Optimal generation scheduling using SAGA for case 1.

Interval	CCGT (MW)	P _{GT2} (MW)	P _{GT3} (MW)	P _{GT4} (MW)	P _{GH1} (MW)	P _{GH2} (MW)	P _{GS} (MW)	P _L (MW)	Q ₁ (m ³ /h)	Q ₂ (m ³ /h)
1	71.05 m ⁴	31.20	18.24	12.97	22.94	11.60	0.00	2.0	258.02	228.89
2	78.92 m ⁴	38.20	21.17	17.02	26.51	16.86	0.00	2.7	290.02	321.49
3	10.62 m ⁴	39.93	15.00	18.42	23.17	33.17	0.00	4.3	260.10	612.33
4	132.28 m ⁴	52.60	0.00	26.74	28.81	33.61	0.00	7.0	310.80	620.28
5	130.26 m ⁴	54.49	15.00	28.80	28.21	32.42	1.00	6.8	305.38	598.82
6	119.02 m ⁴	49.29	23.30	26.54	28.85	28.62	1.98	5.6	311.17	530.74
7	110.97 m ⁴	41.30	25.67	19.43	27.50	22.25	3.44	4.6	298.97	417.10
8	102.65 m ⁴	34.11	21.33	13.91	23.80	14.60	6.20	3.6	265.75	281.69
9	93.38 m ⁴	28.38	17.03	12.28	23.46	11.40	8.94	2.9	262.75	225.42
10	78.59 m ³	20.00	15.00	10.00	18.34	10.00	11.01	1.9	217.03	200.81
11	65.18 m ³	20.00	15.00	10.00	15.48	10.00	12.78	1.4	191.71	200.81
12	74.21 m ³	20.00	15.00	10.00	18.64	10.00	13.93	1.8	219.67	200.81
13	78.66 m ³	20.00	15.00	10.90	22.51	10.20	14.71	2.0	254.22	204.35
14	89.29 m ⁴	24.49	15.00	11.08	22.59	10.00	15.09	2.5	254.96	200.81
15	94.16 m ⁴	31.66	19.68	13.55	24.39	13.27	14.36	3.1	271.06	258.16
16	100.44 m ⁴	38.05	24.47	14.46	27.15	17.65	13.51	3.7	295.79	335.43
17	107.23 m ⁴	40.88	24.18	17.79	27.87	20.85	11.48	4.3	302.31	392.12
18	109.53 m ⁴	40.22	24.58	17.00	26.56	19.04	8.41	4.3	290.49	360.05
19	103.00 m ⁴	39.78	26.91	19.52	28.28	18.79	3.72	4.0	305.97	355.70
20	111.21 m ⁴	37.09	23.23	14.35	25.94	17.32	0.13	4.3	284.99	329.58
21	97.33 m ⁴	34.05	22.10	14.18	24.65	15.04	0.00	3.3	273.35	289.44
22	97.02 m ⁴	27.54	16.10	10.71	22.99	10.64	0.00	3.0	258.53	212.02
23	88.13 m ³	20.00	15.00	10.00	20.22	10.00	0.00	2.3	233.75	200.81
24	96.03 m ³	0.00	0.00	0.00	23.15	14.12	0.00	2.3	259.97	273.16

5.3.3. Case 2: Bitola, Macedonia

The average fuel cost for all sub-cases, obtained using the proposed method, is shown in Table 11, and the computation time taken by the algorithm is 22.14 s. The average fuel costs are obtained from the 50 independent simulations. Figure 12, Figure 13, and Figure 14, respectively, show the optimal output power of TPPs and HPPs for sub-case 1, 2, and 3, while the optimal generation scheduling for the optimization period for the lowest cost sub-case, obtained by newly proposed SAGA, is shown in Figure 14 and in Table 12.

Table 11. Total fuel cost for case 2.

	Sub-Case 1	Sub-Case 2	Sub-Case 3
FT (EUR)	10,397.02	10,345.02	10,184.02
Relative change compared to sub-case 3 (%)	2.05	1.55	-

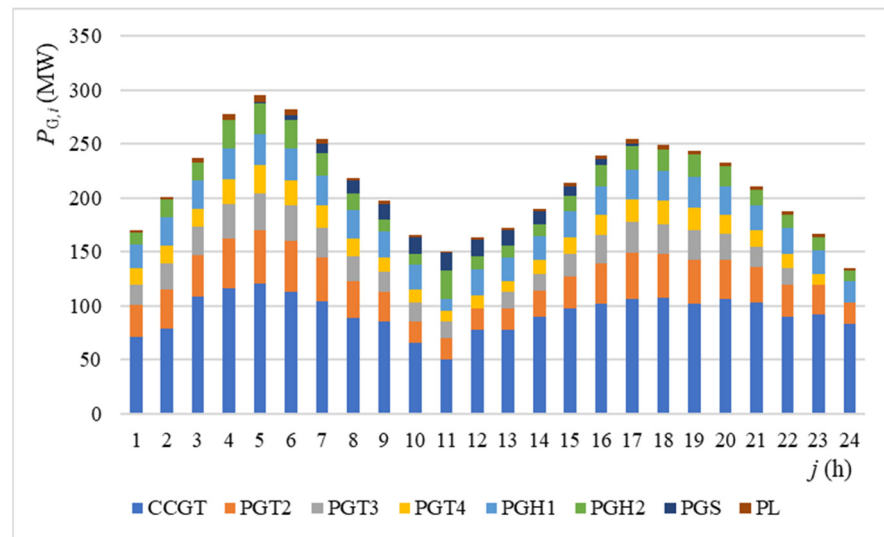


Figure 12. Optimal generation scheduling for case 2-sub-case 1.

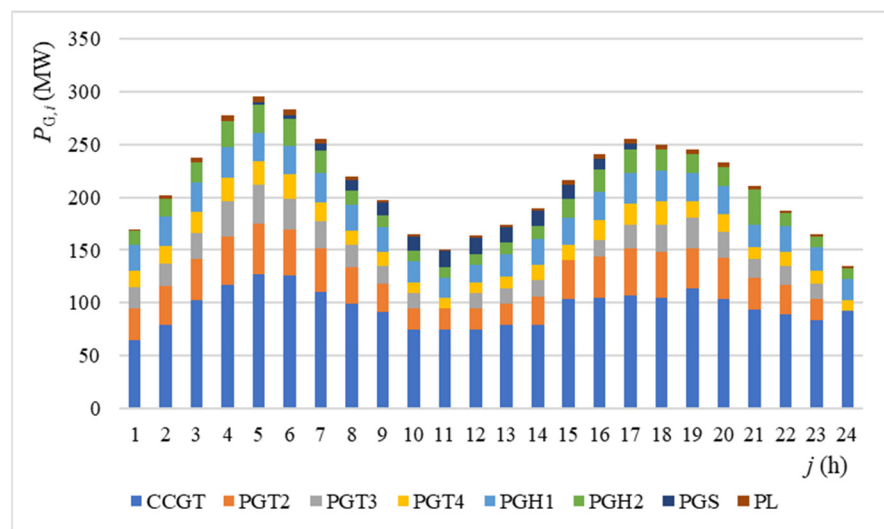


Figure 13. Optimal generation scheduling for case 2-sub-case 2.

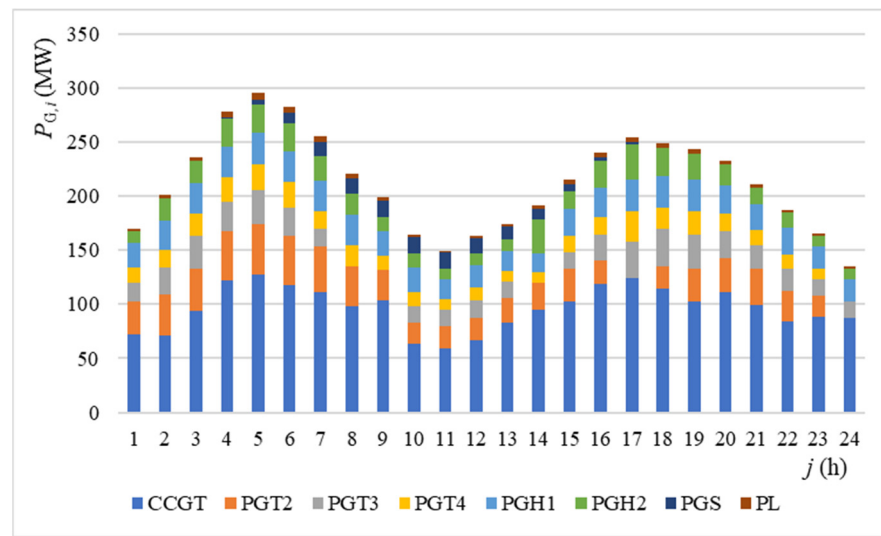


Figure 14. Optimal generation scheduling for case 2–sub-case 3.

Table 12. Optimal generation scheduling using SAGA for case 2.

Interval	CCGT (MW)	P_{GT2} (MW)	P_{GT3} (MW)	P_{GT4} (MW)	P_{GH1} (MW)	P_{GH2} (MW)	P_{GS} (MW)	P_L (MW)	Q_1 (m ³ /h)	Q_2 (m ³ /h)
1	71.68 m ⁴	30.87	17.51	13.99	22.70	11.27	0.00	2.0	255.94	223.06
2	71.09 m ⁴	38.49	24.79	15.85	27.21	21.01	0.00	2.4	296.33	395.08
3	93.38 m ⁴	39.98	29.62	20.81	28.60	20.16	0.00	3.6	308.92	379.87
4	121.68 m ⁴	45.73	27.05	23.00	28.85	26.04	0.17	5.5	311.17	484.57
5	127.31 m ⁴	46.65	32.06	23.50	28.85	26.46	4.54	6.0	311.17	492.11
6	117.57 m ⁴	46.27	25.19	24.05	28.63	25.40	10.17	5.3	309.13	473.13
7	111.55 m ⁴	41.76	16.07	17.03	28.09	23.08	13.01	4.6	304.30	431.72
8	97.86 m ⁴	37.23	0.0	19.33	28.45	19.44	14.46	3.8	307.51	367.21
9	103.39 m ⁴	28.67	0.0	12.44	22.69	13.12	15.16	3.5	255.79	255.52
10	63.04 m ³	20.24	15.00	12.52	23.49	12.67	15.51	1.5	262.97	247.72
11	59.45 m ³	20.00	15.00	10.00	18.30	10.00	15.52	1.3	216.72	200.81
12	67.26 m ³	20.00	16.58	11.22	21.34	10.94	14.24	1.6	243.72	217.30
13	83.41 m ³	22.15	15.00	10.00	19.13	10.00	12.51	2.2	224.02	200.81
14	94.72 m ⁴	25.17	0.00	10.00	17.61	30.48	10.27	3.2	210.51	564.10
15	103.06 m ⁴	29.63	15.00	15.80	24.56	16.21	7.24	3.5	272.52	310.09
16	119.02 m ⁴	20.98	24.35	16.26	27.47	24.54	3.69	4.3	298.69	457.81
17	124.51 m ⁴	0.00	33.45	28.56	28.85	32.97	1.98	4.3	311.17	608.71
18	114.34 m ⁴	20.51	35.20	19.50	28.85	26.44	0.32	4.2	311.17	491.76
19	102.08 m ⁴	30.81	31.35	21.80	28.85	24.91	0.00	3.8	311.17	464.37
20	111.04 m ⁴	31.91	24.55	16.01	26.72	18.87	0.00	4.1	291.92	357.16
21	98.91 m ⁴	34.51	21.27	13.98	24.11	14.63	0.00	3.4	268.57	282.26
22	83.69 m ³	28.58	20.36	13.13	24.92	13.83	0.00	2.5	275.81	268.05
23	88.07 m ³	20.00	15.09	10.00	20.13	10.05	0.00	2.3	232.98	201.63
24	87.82 m ³	0.00	15.00	0.00	20.05	10.00	0.00	1.9	232.23	200.81

5.4. Analysis of the Obtained Results

First of all, the total fuel costs of the test system 1 are EUR 57,640, compared to other previously proposed algorithms, where they are EUR 66,117, EUR 66,121, and EUR 66,198. The same was established for test system 2, which refers to unit commitment, where the total costs amount to EUR 13,126.31, compared to the previously proposed methods, i.e., EUR 13,292.28 and EUR 13,600.00. According to this, it can be concluded that the proposed SAGA provides better results (for all parts, i.e., unit commitment and hydro-thermal scheduling) compared to optimization algorithms proposed in [30,38,39].

For case 1, the sub-case with the lowest total fuels costs is sub-case 2, where they are EUR 10,255.34. For sub-cases 1 and 3, the total fuel costs are EUR 10,316.19 and EUR 10,320.99, which is a relative change, i.e., sensitivity by 0.59% and 0.63%, compared to sub-case 2, which is not a small amount, in terms of short-term planning.

For case 2, the best scenario is sub-case 3, where the total fuel costs are EUR 10,184.02. For the sub-cases 1 and 2, the total fuel costs are EUR 10,397.02 and EUR 10,345.02, which is a relative change, i.e., sensitivity by 2.05% and 1.55%, respectively, compared to sub-case 3, which is also not negligible. The different sensitivities for cases 1 and 2 are based on the fact that these two different locations have significantly different global horizontal solar radiation. The annual global horizontal solar radiation for Gaag, Netherlands is 1040.0 kWh/m², while, for Bitola, Macedonia, it is 1480.3 kWh/m², i.e., even 50 percent higher.

This statement can confirm the initial hypothesis, i.e., that the different orientation of the PV modules affects the total fuel costs in the system. It is important that the different orientation of the PV modules also affects other system parameters, such as active power of transmission lines and optimal output power of TPPs and HPPs, according to Figures 9–14. On the other hand, the auxiliary hypothesis can also be confirmed, i.e., that the different location of the SPP installation also has an impact on the total fuel costs, even for the same topological structure of the system, which is the case in this paper. The confirmation of the hypothesis is also based on the fact that the transmission line constraint has a major impact on fuel costs because it directly affects the optimal power flow of the system. This means that if the active power of one of the transmission lines in a given time interval is equal to its maximum capacity, then the optimal output power from an HPP or TPP (regardless of whether it is the most economical TPP) will be redirected to another transmission line or distributed to several transmission lines. The consequences of this scenario are greater transmission losses and, hence, reduced overall efficiency and increased fuel costs.

In other words, the transmission line constraint limits the production from the “optimal” hydroelectric plant or thermal power plant and forces production from another thermal power plant that may have a higher HR, which significantly affects the overall fuel costs.

On the other hand, the power that the solar power plant injects into the system also has an impact on power flows, but also on TPPs and HPPs. In other words, in some intervals, the output power of the SPP is almost maximum and, in other periods, it is zero. In order to cover such a sudden change, the TPPs are exposed to a sudden change in their output power, i.e., their ramp rate limit is directly affected, and thus to their optimal power, i.e., total fuel costs. In this case, the cost sensitivity of the ramp rate limit is not so pronounced due to the implementation of CCGT in the system. The advantage of CCGT is that it has a negligibly low ramp rate limit, which significantly contributes to maintaining the stability of the system, as well as reducing overall fuel costs.

From all this, another hypothesis can be confirmed. It means that the solution for the SPP installation with an orientation that “covers” the peaks in the electricity price diagram will give the lowest total fuel costs.

6. Conclusions

The optimal generation and optimal power flow in SHTSS are of the most important goals in the planning and operation of modern power systems. The use of power electronic devices and systems expands the possibilities of power regulation and control of power

plants. In this aspect, in recent years, more and more research has focused on the solution of this problem. Unfortunately, in most of the published manuscripts, a number of factors that affect the quality of the obtained results are neglected: CCGT, security constraints (valve point effect, ramp rate, spinning reserve, and transmission line constraint), and power flow calculations. In this sense, this paper focuses on solving the problem of optimal short-term hydrothermal planning in a more realistic manner, i.e., focuses on the application of CCGT and solar power plants in short-term hydrothermal planning. This was achieved by introducing the security and power flow constraints into the SHTSS mathematical model. A novel GA algorithm is proposed that uses a self-adaptive mechanism, LX operator, MPTM operator, adaptive crossover, and mutation strategy to solve the SHTSS problem under an imposed DC power flow constraint. The complex constraints of the SHTSS problem are solved by using a new approach to their handling. The optimization results obtained by using the proposed SAGA algorithm on a known hydrothermal test system are compared with those obtained by other algorithms. The comparisons convincingly proved that the proposed SAGA performs better than other algorithms in terms of both determining the optimal value and the average CPU time used to solve the problem. After verifications of traditional SHTSS problems, SAGA is used for SHTSS problem of IEEE 30 bus systems considering transmission networks, CCGT and SPP. These results also show the better qualities of the proposed SAGA. To better illustrate the impact of different parameters on the final solutions, the proposed constraint handling techniques are neglected and the hydrothermal test system is solved by classical GA. The numerical results obtained from this test system show that LX, MPTM, self-adaptive fitness, and adaptive crossover and mutation strategy also play an important role in the SAGA algorithm. Numerical results show that using these parameters would significantly increase the feasible solutions and reduce the total fuel costs. All this has an extraordinary impact in the current state of the energy crisis and constantly increasing prices of energy carriers.

On the other hand, taking into account the expansion of the share of produced energy from decentralized sources and that, in accordance with the EU directives, there is a tendency towards the gradual decommissioning of thermal power plants, the proposed algorithm can be successfully applied to a hydro-thermal-solar system. Therefore, the proposed metaheuristic algorithm gives a clear picture of the operational planning of the system in the phase of gradual replacement of classical TPPs with combined cycle units (CCGT), but also the growing influence of large SPPs on total fuel costs and overall system parameters.

Possible disadvantages of the proposed algorithm can be the long time required for its modeling, as well as the strong intercorrelation of the proposed techniques that could affect the output parameters. However, keeping in mind the theorem “there is no free lunch”, this should not affect the positive outcomes, such as solving a very complex optimization problem, avoiding local optima, and obtaining a better and more physically realistic solution compared to other methods.

On the other hand, the author performs further research and upgrades to the mathematical model of the proposed algorithm in order to solve the AC short-term hydro-thermal-solar scheduling, i.e., considering voltage bus constraint, reactive power constraint, and reactive power flow limit. This means that the Newton–Raphson’s method will be implemented in the algorithm for power flow solving. This model will enable considering the stochastic nature of SPPs, and objective function will be extended with a penalty function for solar irradiation.

Therefore, the developed algorithm and the presented opportunities for its development allow a much more realistic and physically feasible solution to the SHTSS optimization problem to be obtained. This is also necessary for optimal planning of the operation of the power system from the point of view of investments, energy security, and reliability.

Author Contributions: B.P., N.H., A.I., and D.D. were involved in the full process of producing this paper, including conceptualization, methodology, modeling, validation, visualization, and preparing the manuscript. All authors have read and agreed to the published version of the manuscript.

Funding: This research was funded by Bulgarian National Scientific Fund, grant number KII-06-H57/7/16.11.2021 and the APC was funded by KII-06-H57/7/16.11.2021.

Institutional Review Board Statement: Not applicable.

Informed Consent Statement: Not applicable.

Data Availability Statement: Not applicable.

Acknowledgments: This research was carried out within the framework of the project “Artificial Intelligence-Based modeling, design, control and operation of power electronic devices and systems”, KII-06-H57/7/16.11.2021, Bulgarian National Scientific Fund.

Conflicts of Interest: The authors declare no conflict of interest.

Glossary

Symbols

NT	number of TPPs
NH	number of HPPs
NS	number of SPPs
F	total costs, EUR
$P_{GT,t}$	output power of TPP t , MW
$P_{GH,h}$	output power of HPP h , MW
$P_{GS,s}$	output power of SPP s , MW
P_P	system load, MW
P_L	transmission losses, MW
T_j	duration of interval j , h
J	duration of optimization period, h
R	spinning reserve, MW
$P_{P,max}$	system's peak load, MW
P_G^{min}	unit technical minimum, MW
P_G^{max}	unit technical maximum, MW
B_{ij}, B_{i0}, B_{00}	Crohn's B coefficients for losses
Q_{th}	water discharge of hydro unit h , m ³ /h
$P_{GT,t}^{AV}$	available spinning reserve of TPP t , MW
$P_{GH,h}^{AV}$	available spinning reserve of HPP h , MW
R_T	total required spinning reserve of TPPs, MW
R_H	total required spinning reserve of HPPs, MW
T_{dis}	discharge time, h
URT, URH	up rate of TPP and HPP, MW
DRT, DRH	down rate of TPP and HPP, MW
$P_{GR,g}$	active power of transmission line g , MW
$p_{GR,g}^{max}$	maximum transmission capacity of transmission line g , MW
G	number of transmission lines
$V_{h,k}$	available water volume of HPP h , 10 ³ m ³
$W_{max,i}$	total available energy of generator i , MWh
$V_{h,j}$	storage volume of HPP h at interval j , 10 ³ m ³
$I_{h,j}$	inflow in reservoir h at interval j , 10 ³ m ³
$S_{h,j}$	water spillage of reservoir h at interval j , 10 ³ m ³
V_{h0}, V_{h24}	initial and final volume of reservoir h , 10 ³ m ³
V_h^{min}, V_h^{max}	minimum and maximum volume of reservoir h , 10 ³ m ³
$d(X), p(X)$	distance value and penalty value
$v(X)$	total constraint violation
f_s	scaled fitness function
f_{av}	average fitness function of current population
f_{max}, f_{min}	maximal and minimal fitness function of current population

a_s, b_s	scaling coefficients
β_L, a_L, b_L	LX parameters
x_1, x_2	parent chromosomes
y_1, y_2	children chromosomes
\hat{p}, p, b_m	MPTM parameters
k_1, k_2, k_3, k_4	constants of crossover strategy and mutation strategy
P_c, P_m	crossover probability and mutation probability
g_i, h_k	inequality and equality constraints
Subscripts	
j	hour number
t	TPP index
h	HPP index
g	transmission line index
m	gene index
n	chromosome index
i	inequality constraint index
k	equality constraint index
Abbreviations	
SHTSS	short-term hydro-thermal-solar scheduling
SAGA	self-adaptive genetic algorithm
LX	Laplace crossover
MPTM	Makinen, Periaux, and Toivanen mutation
UC	Unit Commitment

References

- Braun, S. Improving Flexibility of Fossil Fired Power Plants. *Encycl. Energy Storage* **2022**, *2*, 133–140.
- Zhao, X.; Yin, H.; Zhao, Y. Impact of environmental regulations on the efficiency and CO₂ emissions of power plants in China. *Appl. Energy* **2015**, *149*, 238–247. [[CrossRef](#)]
- Schreiber, A.; Zapp, P.; Kuckshinrichs, W. Environmental assessment of German electricity generation from coal-fired power plants with amine-based carbon capture. *Int. J. Life Cycle Assess.* **2009**, *14*, 547–559. [[CrossRef](#)]
- Singh, R.; Banerjee, R. Impact of large-scale rooftop solar PV integration: An algorithm for hydrothermal-solar scheduling (HTSS). *Sol. Energy* **2017**, *157*, 988–1004. [[CrossRef](#)]
- Libal, J.; Kopecek, R. *Bifacial Photovoltaics: Technology, Applications and Economics*, 1st ed.; IET: London, UK, 2018; pp. 153–220.
- Tang, J.; Luh, P.B. Hydro thermal scheduling via extended differential dynamic programming and mixed coordination. *IEEE Trans. Power Syst.* **1995**, *10*, 2021–2028. [[CrossRef](#)]
- Jin-Shyr, Y.; Nanming, C. Short term hydro thermal coordination using multi pass dynamic programming. *IEEE Trans. Power Syst.* **1989**, *4*, 1050–1056. [[CrossRef](#)]
- Guan, X.; Ni, E.; Li, R.; Luh, P.B. An optimization-based algorithm for scheduling hydro thermal power systems with cascaded reservoirs and discrete hydro constraints. *IEEE Trans. Power Syst.* **1997**, *12*, 1775–1780. [[CrossRef](#)]
- Al-Agtash, S. Hydro thermal scheduling by augmented lagrangian: Consideration of transmission constraints and pumped storage units. *IEEE Trans. Power Syst.* **2001**, *16*, 750–756. [[CrossRef](#)]
- Nilsson, O.; Sjelvgren, D. Mixed integer programming applied to short term planning of a hydro thermal system. *IEEE Trans. Power Syst.* **1996**, *11*, 281–286. [[CrossRef](#)]
- Maturana, J.; Riff, M.C. Solving the short-term electrical generation scheduling problem by an adaptive evolutionary approach. *Eur. J. Oper. Res.* **2007**, *179*, 677–691. [[CrossRef](#)]
- Wong, D.P.; Wong, Y.W. Short term hydro thermal scheduling part. I. Simulated annealing approach. *IEE Proc.-Gener. Transm. Distrib.* **1994**, *141*, 497–501. [[CrossRef](#)]
- Jayabarathi, T.; Chalasani, S.; Shaik, Z.A. Hybrid differential evolution and particle swarm optimization-based solutions to short term hydro thermal scheduling. *WSEAS Trans. Power Syst.* **2007**, *2*, 245–254.
- Diew, V.N.; Ongsakul, W. Enhanced merit order and augmented Lagrange Hopfield network for hydro thermal scheduling. *Int. J. Electr. Power Energy Syst.* **2008**, *30*, 93–101.
- Gil, E.; Bustos, J.; Rudnick, H. Short term hydrothermal generation scheduling model using genetic algorithm. *IEEE Trans. Power Syst.* **2003**, *18*, 1256–1264. [[CrossRef](#)]
- Titus, S.; Jeyakumar, A.E. Hydrothermal scheduling using an improved particle swarm optimization technique considering prohibited operating zones. *Int. J. Soft Comput.* **2007**, *2*, 313–319.
- Liu, C.; Shahidehpour, M.; Li, Z.; Fotuhi-Firuzabad, M. Component and Mode Models for the Short-Term Scheduling of Combined-Cycle Units. *IEEE Trans. Power Syst.* **2009**, *24*, 976–990.
- General Electric GE Power. Combined Cycle Power Plant. Available online: www.ge.com/power/resources/knowledge-base/combined-cycle-power-plant-how-it-works (accessed on 14 July 2022).

19. Kehlhofer, R.; Rukes, B.; Hannemann, F.; Stirnimann, F. *Combined-Cycle Gas & Steam Turbine Power Plants*, 3rd ed.; PennWell: Tulsa, OK, USA, 2009; pp. 35–68.
20. Postolov, B.; Iliev, A. New metaheuristic methodology for solving Security Constrained Hydrothermal Unit Commitment based on Adaptive Genetic Algorithm. *Int. J. Electr. Power Energy Syst.* **2022**, *134*, 107163. [[CrossRef](#)]
21. Zhu, J. *Optimization of Power System Operation*, 2nd ed.; Wiley-IEEE Press: Hoboken, NJ, USA, 2015; pp. 297–346.
22. Soliman, A.; Mantawy, A.H. *Modern Optimization Techniques with Applications in Electric Power Systems*, 1st ed.; Springer: New York, NY, USA, 2012; pp. 83–280.
23. Ongsakul, W.; Vo, D.N. *Artificial Intelligence in Power System Optimization*, 1st ed.; CRC Press: New York, NY, USA, 2013; pp. 118–314.
24. Postolov, B.; Iliev, A. Adaptive Genetic Algorithm for Hydro-thermal Unit Commitment Considering the Security Constraints. *Int. J. Electr. Eng. Comput.* **2020**, *4*, 61–69. [[CrossRef](#)]
25. Michalewicz, Z. *Genetic Algorithms + Data Structures = Evolution Programs*, 3rd ed.; Springer: New York, NY, USA, 1996; pp. 283–314.
26. Deb, K. An efficient constraint handling method for genetic algorithms. *Comput. Meth. Appl. Mech. Eng.* **2000**, *186*, 311–338. [[CrossRef](#)]
27. Qin, A.K.; Huang, V.L.; Suganthan, P.N. Differential evolution algorithm with strategy adaptation for global numerical optimization. *IEEE Trans. Evol. Comput.* **2009**, *13*, 398–417. [[CrossRef](#)]
28. Mallipeddi, R.; Suganthan, P.N. Ensemble of constraint handling techniques. *IEEE Trans. Evol. Comput.* **2010**, *14*, 561–579. [[CrossRef](#)]
29. Farmani, R.; Wright, J.A. Self-adaptive fitness formulation for constrained optimization. *IEEE Trans. Evol. Comput.* **2003**, *7*, 445–455. [[CrossRef](#)]
30. Tessema, B.G.; Yen, G.G. A Self Adaptive Penalty Function Based Algorithm for Constrained Optimization. In Proceedings of the IEEE International Conference on Evolutionary Computation, Vancouver, BC, Canada, 16–21 July 2006.
31. Sivanandam, S.N.; Deepa, N. *Introduction to Genetic Algorithms*, 1st ed.; Springer: Berlin, Germany, 2008; pp. 83–122.
32. Kramer, O. *Genetic Algorithm Essentials*, 1st ed.; Springer International Publishing: Cham, Switzerland, 2017; pp. 11–28.
33. Bansal, J.C.; Singh, P.K.; Pal, N.R. *Evolutionary and Swarm Intelligence Algorithms*, 1st ed.; Springer International Publishing: Cham, Switzerland, 2019; pp. 61–85.
34. Deep, K.; Thakur, M. A new crossover operator for real coded genetic algorithms. *Appl. Math. Comput.* **2007**, *188*, 895–911. [[CrossRef](#)]
35. Makinen, R.A.E.; Periaux, J.; Toivanen, J. Multidisciplinary shape optimization in aerodynamics and electromagnetic using genetic algorithms. *Int. J. Numer. Methods Fluids* **1999**, *30*, 149–159. [[CrossRef](#)]
36. Basu, M. Artificial immune system for fixed head hydrothermal power system. *Energy* **2011**, *36*, 606–612. [[CrossRef](#)]
37. Postolov, B.; Iliev, A.; Dimitrov, D.; Dimishkoska, N. N-1 Security Constrained Short-Term Hydrothermal Scheduling by Self Adaptive Genetic Algorithm with PTDF. In Proceedings of the 2021 International Conference on Information Technologies (InfoTech), Varna, Bulgaria, 16–17 September 2021; pp. 1–7.
38. Khunkitti, S.; Watson, N.R.; Chatthaworn, R.; Premrudeepreechacharn, S.; Siritaratiwat, A. An Improved DA-PSO Optimization Approach for Unit Commitment Problem. *Energies* **2019**, *12*, 2335. [[CrossRef](#)]
39. Kamboj, V.K. A novel hybrid PSO–GWO approach for unit commitment problem. *Neural Comput. Appl.* **2016**, *27*, 1643–1655. [[CrossRef](#)]
40. Bouchekara, H.R.E.H.; Chaib, A.E.; Abido, M.A.; El-Sehiemy, R.A. Optimal Power Flow Using an Improved Colliding Bodies Optimization Algorithm. *Appl. Soft Comput.* **2016**, *42*, 119–131. [[CrossRef](#)]
41. Aghdam, F.H.; Hagh, M.T. Security Constrained Unit Commitment (SCUC) formulation and its solving with Modified Imperialist Competitive Algorithm (MICA). *J. King Saud Univ.-Eng. Sci.* **2019**, *31*, 253–261. [[CrossRef](#)]
42. Surekha, P. Investigation of Efficient Bio Inspired Intelligent Paradigms for Solving Unique Constraint Based Optimization Problems. Ph.D. Thesis, Anna University, Chennai, India, 1 August 2014.
43. Nguyen, T.T.; Vo, D.N.; Truong, A.V.; Ho, L.D. Meta-Heuristic Algorithms for Solving Hydrothermal System Scheduling Problem Considering Constraints in Transmission Lines. *Glob. J. Technol. Optim.* **2016**, *7*, 1000192.
44. Lu, B. Short-Term Scheduling of Combined Cycle Units. *IEEE Trans. Power Syst.* **2004**, *19*, 1616–1625. [[CrossRef](#)]
45. Trinasolar. PV Modules Vertex 500W TSM-DEG18MC.20(II) Bifacial, 1/3-Cut, MBB, 485-505W. Available online: <https://www.trinasolar.com/en-glb/product/VERTEX-DEG18MC20II> (accessed on 14 July 2022).
46. HUPX. Historical Data. Available online: <https://hupx.hu/en/market-data/dam/historical-data> (accessed on 14 July 2022).